Check for updates

Ultrasensitive and label-free detection of prognostic and diagnostic biomarkers of sepsis on a AgNP-laden black phosphorous-based SERS platform†

Anirban Kundu, [iD] Renu Rani, Anas Ahmad, [iD] Ajay Kumar, Mamta Raturi, Tanya Gupta, Rehan Khan [iD]* and Kiran Shankar Hazra [iD]*

Rapid and early detection of sepsis biomarkers is essential and an immediate need to prevent significant casualties of ICU patients caused by an uncontrolled infection in the patient's body. A highly sensitive and selective surface-enhanced Raman spectroscopy (SERS) based detection protocol has been established to detect the sepsis biomarkers. For this purpose, uniquely designed SERS substrate on black phosphorus (BP) flake are fabricated by a one-step and straightforward process where uniform silver nanoparticles (AgNPs) are synthesized over the BP surface, which in turn enhance the stability of BP flakes. Both the prognostic [interleukin-3 (IL-3)] and diagnostic [procalcitonin (PCT)] biomarkers are detected up to a limit of detection (LOD) as low as 1000 fM and 100 fM, respectively, where the SERS enhancement factor (EF) is obtained as high as in the order of $\sim 10^{14}$. A comprehensive study of Raman spectra has been carried out to explore the origin of observed Raman peaks of IL-3 and PCT, arising from various amino acids, which has never been reported earlier. The unknown signature Raman peaks for such biomarkers are identified at low energy regions, occurring due to structural variation of the two different protein chains even though both consist of the same possible amino acids. The findings of signature Raman modes of sepsis biomarkers help distinguish the Raman peaks of sepsis biomarkers in spiked clinical samples even in the simultaneous presence of both the biomarkers.

Introduction

Sepsis affects about 30 million humans globally and is the leading cause of death of ICU patients worldwide due to its complicated detection techniques and the absence of prompt treatment.[1,2] Sepsis is a severe inflammatory reaction to infectious agents, and readily advances to a sustained immunosuppressive condition. Thus, it has become the reason for significant mortality rates.[3] Sepsis requires immediate medical treatment to avoid casualties within hours of the disease onset due to its rapid growth of infection in the body. This leads to the condition of organ failure, termed as *septic shock*.[4] Various pathogens, such as bacteria, fungi or viruses, can cause sepsis, but most of the sepsis cases are caused by bacterial infections.[5] Sepsis is also observed as a common complication directly caused by the new coronavirus (SARS-CoV2) first reported in late 2019.[6,7] The optimized sepsis management requires the rapid, early and sensitive detection of various diagnostic and prognostic sepsis biomarkers, which can be diagnosed on a single platform. However, such kinds of detection and diagnostic techniques are still rarely accessible and create significant lacunae in the timely management of the pathophysiological consequences of sepsis.[8,9] Rapid and accurate detection has also become significant as it helps in the well-timed administration of appropriate antimicrobial agents that potentially obviate the attainment of critical septic stages, and can thus prevent fatalities.[10]

Techniques, like enzyme-linked immunosorbent assay (ELISA), polymerase chain reaction (PCR), fluorescence *in situ* hybridization (FISH), microarray hybridization and proteomics spectrometry phage assays,[11-14] are available for the detection of sepsis. However, they have limitations due to their selectivity and longer process time in the typical range of 12 hours to few days.[15] Since the affected patients have a rapid progression of underlying infection, the level of most of the biomarkers shoots up during the standard testing duration, which disables the identification of the real-time infection stage. In recent years, serum biomarkers, such as C-reactive protein (CRP), tumor necrosis factor-alpha (TNF-α), interleukin-6 (IL-6), and Fc-gamma receptor-1 (FcγR1) (also called CD64), have been explored to identify the progress and

Institute of Nano Science and Technology, Knowledge City, Sector 81, Mohali, Punjab, 140306, India. E-mail: rehankhan@inst.ac.in, kiran@inst.ac.in

Communication

Sensors & Diagnostics

Table 1 Sepsis biomarkers and their detection techniques

Phase	Category	Markers	Type	Method	Process time
Hyper-inflammatory	Cytokines	TNF-α, IL-1β, IL-6	Prognostic	Immunoassay[61]	2–5 days
	Chemokines	IL-8, IL-10	Diagnostic	ELISA[62]	2–5 days
	Protein	CRP, procalcitonin (PCT)	Diagnostic	ELISA[17]	2–5 days
	Complementary peptides	C3b, C5a	Diagnostic	ELISA[63]	2–5 days
	Antigens on neutrophils and monocytes	CD64, CD11b, CD14	Diagnostic	Flow cytometry; immunoassay[64]	3–6 hours; 2–5 days
	Detection of microbes	RNA	Diagnostic	PCR[65]	2–5 days
Immuno-suppressive	Surface antigens	↓MHC II, ↓CD28, ↑CD152 (CTLA) IL-10	Diagnostic	ELISA[66]	2–5 days
Organ dysfunction	Proteins	↑lactate, IL-6, PCT, fibrinolysis (↑coagulation factors)	Diagnostic	Immunoassays, DIC (disseminated intravascular coagulation) score for fibrinolysis[17]	2–5 days; over hours or days

prediction of the sepsis.[10,13,16–18] However, the desired selectivity and sensitivity of these techniques for early detection are not adequate. The absence of a specific treatment and the complicated pathogenesis of sepsis make it necessary for the early detection of disease biomarkers, so that supportive medications can be implemented at an early stage when it is easily manageable.

Among several biomarkers of sepsis, lipopolysaccharide (LPS) has proven to be an essential mediator in the pathogenesis of Gram-negative bacterial sepsis, which is associated with several other clinical manifestations, like hypertension, blood clotting, diarrhea, pyrogenic reactions, and infections of Gram-negative bacteria such as

meningococcus.[19–21] There is no single ideal biomarker of sepsis present that helps to identify critically ill patients who need immediate medical attention with possible diagnosis and treatment. The category of different sepsis biomarkers and their detection techniques are mentioned in Table 1, which gives an idea about the detection process and required time. Recently, Weber *et al.* identified interleukin-3 (IL-3), a cytokine, as a prognostic biomarker or independent predictor of septic shock and death.[22] Furthermore, Min *et al.* showed that when using a hybrid magneto-electrochemical sensor, the limit of detection (LOD) for IL-3 can be achieved up to <10 pg ml^{-1}, which produces the test results within 1 h.[23] Along with the prognostic biomarker IL-3, the diagnostic
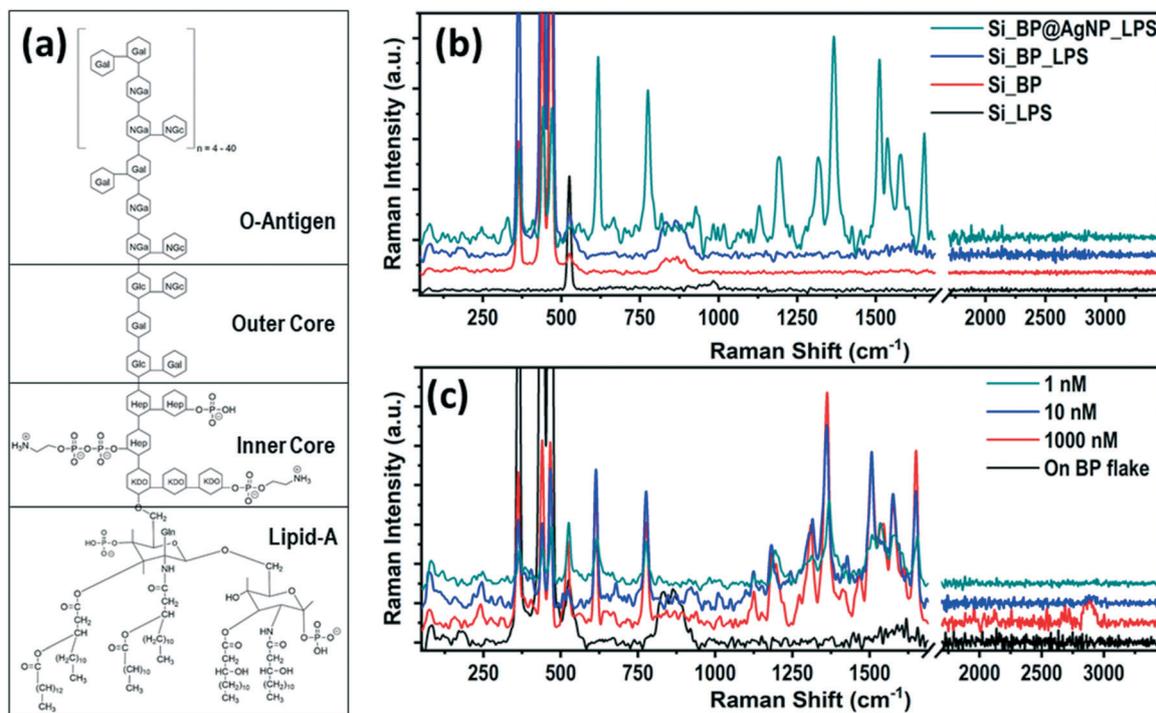
Fig. 1 (a) Chemical structure of lipopolysaccharide (LPS); (b) Raman spectra of LPS on different substrates showing the strong enhancement in the Raman signal only on the AgNP@BP flake; (c) SERS Raman signal of LPS with the variation in the LPS concentration ranging 1000 nM to 1 nM.
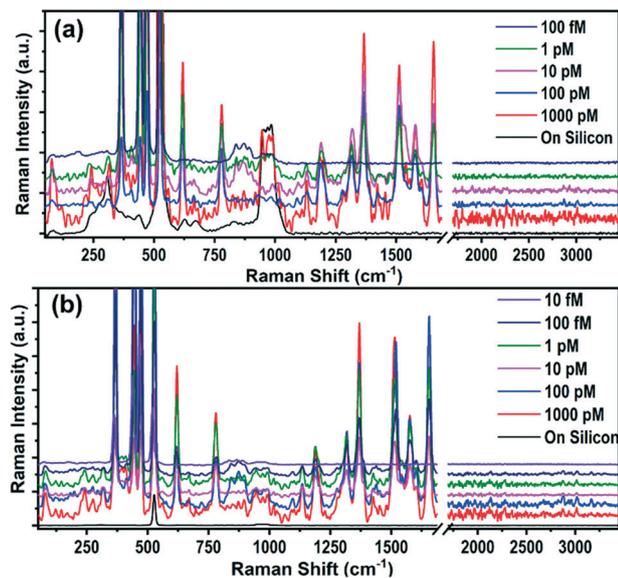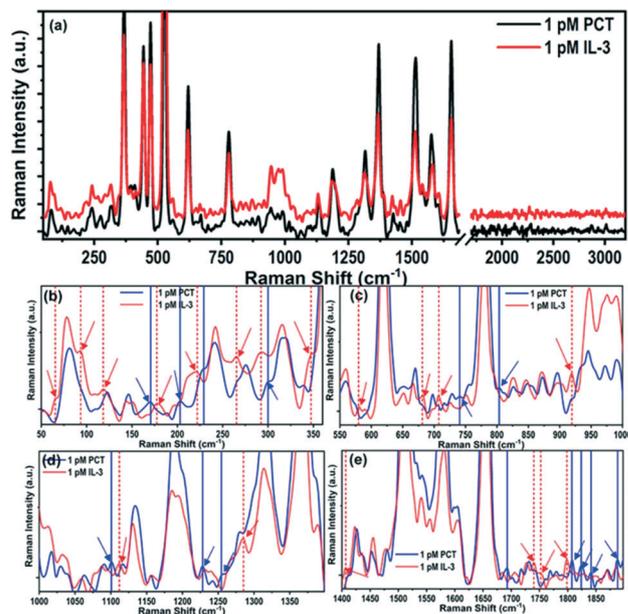
Fig. 2 SERS enhanced Raman spectra of (a) interleukin-3 (IL-3) for different concentrations ranging from 1000 pM to 1 pM; and (b) procalcitonin (PCT) for concentrations from 1000 pM to 10 fM. Intensities of the PCT Raman spectra for 1 pM, 100 fM and 10 fM are multiplied by a factor of 20 for better visibility.

Fig. 3 Observation of signature Raman modes of IL-3 and PCT. (a) Comparative Raman spectra of IL-3 and PCT; (b–e) the Raman spectra have been compared for different energy ranges (b) 50–360 cm^{-1}, (c) 550–1000 cm^{-1}, (d) 1000–1400 cm^{-1} and (e) 1400–1900 cm^{-1}. All of the signature Raman peaks are highlighted for better visualization.

biomarker procalcitonin (PCT) has a vital role in determining the severity of sepsis at different stages. The role of PCT for determining the stage of sepsis has already been proven and explained in several reports.[24–26]

In recent times, 2D layered material-based SERS substrates have emerged as a potential tool for the identification of various biomarkers present in blood or serum. This is due to their advantages of having improved sensitivity, reusability, enhanced stability, stronger surface adsorption capability, and feasible scalability.[27–29] Reports show that the graphene and MoS$_2$-based SERS platform has application in bio-sensing for the sensitive detection of diseases, like bacterial infections,[30] malaria,[31] diabetes,[32] cardiovascular,[33] and brain tumors.[34] However, the SERS signal enhancement of such systems mostly relies on charge transfer between the 2D van der Waals (vdW) nano-sheet/flake and the analyte, rather than the electromagnetic field enhancement.[35] Very recently, layered black phosphorus (BP) has emerged as one of the most suitable 2D materials for SERS applications, as it has intrinsic in-plane ferroelectricity unlike other 2D members, which is favorable for SERS signal enhancement. The laser-induced nano-structuring of the BP flake can create arrays of hotspots, which has emerged as a metal-free SERS substrate.[36] Along with the pristine layered BP flake and its nanostructures, the BP-metal nanoparticle heterostructures have also emerged as a potential platform that can be used for the detection of biomolecules, where the intrinsic biocompatibility of layered BP can be an added advantage.[36–38] In recent times, the heterostructures of the layered BP flake and metal nanoparticles have proved to be a stable and potential platform for the development of bio-

sensors.[38–42] Although the SERS-based detection is precise to the target analyte and capable of ultra-low detection limits,[43,67–69] very little effort has been made so far on the detection of sepsis biomarkers due to the fact that the signature Raman modes of these biomarkers are still unexplored. Although a recent report by Cao *et al.*[44] demonstrated the SERS-based diagnosis for sepsis biomarkers of the C-reactive protein (CRP), procalcitonin (PCT), the limit of detection (LOD) was still only achieved in the range of hundred pM, where the sensitivity may not reach the required level. In such labeled detection technique, no signature Raman modes of the sepsis biomarkers have been identified, which is essential and a primary need for the SERS-based detection technique. Thus, the absence of any label-free detection of prognostic and diagnostic biomarkers of sepsis on a single platform with minimum processing time is a vital necessity to ease the timely detection and management of septic patients.

Here, the ultrasensitive detection of prognostic and diagnostic biomarkers of sepsis is demonstrated using a uniquely designed BP-based SERS substrate. The possible signature Raman modes of the IL-3 and PCT protein chains are distinguished by the Raman signals arising from the amino acid building blocks of IL-3 and PCT. *In situ* growth of silver nanoparticles (AgNPs) over the BP flake is demonstrated, where BP itself acts as a precursor to achieving the uniform distribution of the AgNPs over the BP flake surface. The as-grown AgNPs were used as hotspots for local electric field enhancement in order to obtain enhanced Raman signal of the biomarkers, *i.e.*, LPS, IL-3, and PCT,

Table 2 Raman peak positions, band assignment, and origin of Raman modes for interleukin-3 (IL-3) and procalcitonin (PCT)[59–61]

Wavenumber (cm^{-1})		Band assignment	Reported band position (cm^{-1})	Amino acid[a]
PCT	IL-3			
81.89	79.11			
—	111			
122.52	—			
—	130.11			
144.97	144.39			
169.53	170.63	Lattice stretching	166	W
—	192.36	C–O torsional	185	V
202.76	206.7	Torsional CH$_2$–CH	200–210	C
—	269.06	Torsional	262	M
275.78	—			
300.11	304.8	CCC beading	300	S
—	406.54	Bending N–C–C	400	AY
444.39	445.36	Torsional NH$_3$	450	TP
476.5	476.34	Torsional NH$_2$	475–480	AQ
		Rocking COO	493	T
—	516.53	Rocking COO	515	S
—	535.36	Rocking of COO	530–535	ARI
		COO rocking	544	H
559.72	—	Wagging COO	565	T
		Bending COO	564	Q
		COO rocking	556	I
620.22	618.57	Bending of COO	611	SF
		Amide bending	632	Q
—	647.27	Bending of COO	655–660	AR
		Symmetric C–S stretching	645	MQ
669.2	666.59	COO scissoring	684	H
—	726.87	Torsional COH	703	T
		C–S–C stretching	721	M
—	744.11	CH$_2$ rocking	740–775	CM
		Condensed ring system	757	W
		C–H twisting	749	I
779.81	779.51	OOP of COO	776	T
		COO deformation	782	V
		CNH stretching	784	R
—	794.06	COO bending	804	V
—	840.01	C–C stretching	848	HRNFPI
		Wagging of H at imidazole ring	854	H
		COO OOP	838	L
		Ring breathing vibration	854	Y
—	872.54	Stretching C–C–N	878	T
		C–C stretching	877	ME
		N–H stretching	875	W
—	886.03			
896.39	904.63	NH$_2$ bending	896	P
		NH$_2$ bending	908	R
930.37	—	Stretching C–C	930	TLSD
		C–C asymmetric bending	922	I
972.56	—	C–C stretching	900–970	VH
		CH$_2$ rocking	970	S
991.76	986.61	S–H in-plane bending	990	C
1016.7	1013.1	C–N stretching	1010	S
		Ring breathing	1003	FW
		CC stretching	1008	Q
1033.54	—	OH bending	1032	R
		C–N stretching	1033	LKN
		In-plane bending	1032	F
1096.63	1098.19	Symmetric stretching CN	1091	HRLMQI
		C–O stretching	1090	S
		Rocking NH$_3$	1101	N
1134.67	1130.92	NH$_3$ asymmetric rocking	1140	CLSKQE
		Rocking NH$_3$	1113	H
		Stretching asymmetrical C–C–N	1114	T
		CH$_3$ rocking	1125–1200	V
		Ring deformation of tyrosine	1128	Y

Table 2 (continued)

Wavenumber (cm⁻¹) PCT	IL-3	Band assignment	Reported band position (cm⁻¹)	Amino acid[a]
1187.54	1182.04	NH$_3$ rocking	1175	L
		C–H stretching	1175	M
		NH$_3$ rocking	1188	L
—	1194.24	CH$_2$ twisting	1200	C
		Rocking NH$_3$	1202	T
		CO stretching	1192	R
1279.15	1288.21	CH$_2$ twisting	1265	M
		CH$_2$ bending wagging	1261	Q
1316.53	1317.14	COO stretching	1321	K
		C–H stretching	1311	ED
	1360.42	COO symmetric stretching	1350	C
		C–H twisting	1360	K
		Stretching CH	1358	NQI
		Bending CH	1349	TL
		Pyrrole ring stretching	1359	W
1371.01	1368.3	OH bending	1378	P
1435.9	1423.3	Stretching asymmetric C–O–O	1420	TH
		Stretching CH$_2$	1425	NQED
		Pyrrole ring stretching	1426	W
—	1477.49	Bending CH$_3$	1465	T
		CH$_3$ bending	1400–1460	VRI
		CH stretching (asym)	1465	M
1513.74	1513.3	Asymmetric stretching COO	1506	H
1543.33	1551.32	Benzene ring stretching	1557	W
1577.19	1577.99	OH bending	1544	R
		CC stretching	1586	F
1603.9	—	NH$_3$ bending	1609	K
		CC ring stretching	1604	FY
—	1650.98	Stretching CO	1640	N
1654.72	1655.69	Stretching CO	1692	D

[a] A: alanine; R: arginine; N: asparagine; D: aspartic acid; C: cysteine; Q: glutamine; E: glutamic acid; G: glycine; H: histidine; I: isoleucine; L: leucine; K: lysine; M: methionine; F: phenylalanine; P: proline; S: serine; T: threonine; W: tryptophan; Y: tyrosine; V: valine.

where the detection limit was investigated to as low as ~10 fM.

Experimental details

Materials used

Single crystal of black phosphorus (BP) from Manchester Nanomaterials (MN), UK; lipopolysaccharide (LPS) and silver nitrate (AgNO$_3$) were purchased from Sigma Aldrich, and used without further modification. Human IL3/IL-3 protein (IL-3) and human procalcitonin/CALCA (PCT) were purchased from Sino Biological Inc. Purified human serum IgA was purchased from MP Biomedicals (Catalogue No. 0855979). No study was performed directly on humans and no blood or serum was isolated from any human subject.

Preparation of the AgNP@BP SERS platform

Pristine BP flake was mechanically exfoliated from a bulk BP single crystal on top of a silicon substrate using the standard micromechanical exfoliation technique *via* the scotch-tape method. Few layered-BP flakes were identified in an optical microscope and characterized by a WITec alpha 300R Raman spectrometer, followed by AFM measurement using Bruker

Multimode 8 atomic force microscope (AFM) in tapping mode. The as-exfoliated BP flake supported by the silicon substrate was immersed in the AgNO$_3$ precursor solution with varying concentrations and kept at ~90 °C for ~5 min. The as-fabricated AgNP@BP flake was characterized by Raman spectroscopic measurement and AFM techniques. All of the Raman spectra were recorded in a back-scattering configuration with a Nd:YAG 532 nm laser line using a 100× objective, where the laser power was kept at ~2 mW to avoid the possibilities of chemical alteration of the molecules by laser heating. The SERS EF was calculated by considering the Raman spectra of the PBS buffer solution on the AgNP@BP flake as reference spectra.

TEM sample preparation

Liquid exfoliation of a tiny piece of single-crystal BP was performed by sonication in NMP for 12 h. The exfoliated BP flakes were immediately used for TEM sample preparation by drop-cast on a Cu-grid with 300 mesh, followed by optical microscope identification and Raman measurement. The Cu-grid with the layered BP flake was used for TEM analysis. The same was further used for the deposition of AgNPs as described earlier. The same grid was also further used for

TEM analysis of the AgNP@BP flake. The TEM micrographs were recorded using a JEOL JEM2100 transmission electron microscope with 200 kV accelerating voltage.

Preparation of IL-3 and the PCT solution in PBS

To prepare different concentrations of the biomarkers, the IL-3 and PCT were diluted in phosphate-buffered saline (PBS) solution at pH 7.4.

Preparation of IL-3 and the PCT solution in sterile human serum

Different concentrations of interleukin-3 (IL-3) and procalcitonin (PCT) biomarkers were prepared as spiked samples using sterile human serum. Briefly, the known amounts of IL-3 and PCT were dissolved in sterile PBS solution at pH 7.4 to prepare the final concentrations of the spiked samples in the fM range (10 fM–100 nM). The samples were cooled at 4 °C and then gently stirred over vortexing to obtain a homogenous solution, where a range of six to seven spiked samples were selected for biomarker detection.

Results and discussion

The BP flakes were mechanically exfoliated on a Si substrate, using the standard scotch tape technique and immediately immersed in an aqueous $AgNO_3$ precursor solution for 5 min at 90 °C to avoid any oxidation. Lone pair electrons of phosphorus atoms, evenly distributed all over the BP surface, interacted with the $AgNO_3$ precursor solution to adsorb Ag^+ ions on its surface by reducing Ag^+ to Ag^0.[45] Due to such spontaneous adsorption of the Ag^+ ions on the BP flake by passivating the lone pair electrons, the BP flake surface became stable even under ambient conditions (room temperature ~25 °C and relative humidity ~60%) as compared to the pristine one, which surpassed one of the significant limitations of BP for its practical application.[46,47] The detailed synthesis protocol and characterization of the AgNP-decorated BP flake are described in the ESI† (Fig. S1–S4). The stability of the AgNP-decorated BP (AgNP@BP) flake was examined by AFM (Fig. S5†), where no signs of physical degradation were observed as the thickness, and surface roughness of the flake remained unchanged for up to 72 h under ambient conditions (room temperature ~25 °C and relative humidity ~60%).

The SERS capability of the designed AgNP@BP substrate for the detection of LPS was investigated, where 10 μL solution of LPS with concentrations varying from 1000 nM to 1 nM were drop-casted onto the SERS substrate to conduct Raman spectroscopic measurements. A low laser power of ~2 mW was used to avoid the possibilities of chemical alteration of the molecules by laser heating. LPS is a bacterial endotoxin present in the outer cell membrane of Gram-negative bacteria. It is thought to be a key mediator for the pathogenesis of septic shock.[17] The LPS structure can be divided into three distinct parts, *i.e.*, hydrophobic lipid-A, hydrophilic polysaccharide chain, and the repeating units of the bacterial serotype specific O-antigen oligosaccharide (hydrophilic),[21] as shown in Fig. 1a. Fig. 1b compares the Raman spectra of LPS (concentration ~1 μM) on different substrate configurations (*i.e.*, bare Si, pristine BP on Si, and AgNP@BP on Si), concluding that the signature peaks of LPS arises only on the AgNP@BP SERS substrate due to signal enhancement. In contrast, the peaks at 362, 442, and 465 cm^{-1} originated from the BP flake, which corresponds to the out-of-plane vibration, in-plane armchair and zigzag vibration, respectively, and the peak at 521 cm^{-1} denotes the first order Si Raman mode. The enhancement in the Raman signal is attributed to the increase in the local electric field by the plasmonic effect of the AgNPs decorated on the BP flake. The uniform size and spatial distribution of the nanoparticles with higher density are the key factors for superior SERS enhancement. Here, the electromagnetic enhancement is dominated over the chemical enhancement for contribution towards a higher SERS enhancement factor. Table ST2, in the ESI,† summarizes the observed Raman peaks from LPS and identifies their origins from the specific vibration modes, which has unexplored so far. The signature Raman peaks of LPS are observed at 1131, 1366, and 1655 cm^{-1}, which originated from the presence of lipids[48] in the LPS structure. A Raman peak at 1316 cm^{-1} confirms the presence of aliphatic molecules, whereas the 1579 cm^{-1} peak originates from graphitic carbon. However, the only Raman peak in the high energy range at ~2900 cm^{-1} originated from the C=O and CH_3 stretching modes, which confirms the presence of sugar, lipid and a polyethylene group in the structure.[49]

The SERS signal of LPS for different concentrations (1000–1 nM) are shown in Fig. 1c, where the Raman intensity decreases with the decrease in the LPS concentration. The enhancement in the Raman signal of LPS is not prominent beyond ~1 nM concentration, which is the limit of detection (LOD) of the AgNP@BP SERS substrate for LPS as an analyte. The SERS enhancement factor (EF) for LPS was calculated using the two most intense Raman peaks at 1366 cm^{-1} and 1655 cm^{-1}. The enhancement factor was calculated for different LPS concentrations, which is provided in Table ST4 of the ESI.† The enhancement factor of the reported SERS substrate was calculated from the average area covered by the particles (hotspot area) and the possible number of molecules present at the hotspot vicinity (additional details are provided in the ESI† Fig. S7). The average value of the SERS enhancement factor was found to be surprisingly high, EF ~2.9×10^{14}, for LPS under 532 nm laser excitation.

Although an elevated LPS with LOD of 1 nM could be a good *prima facie* evidence, it cannot be a confirmatory biomarker for the diagnosis of sepsis due to the lack of specificity towards sepsis. Hence, it requires the sensitive detection of more specific biomarkers such as IL-3 (prognostic) and PCT (diagnostic). The Raman spectra of IL-3 and PCT are depicted in Fig. 2a and b, where it is evident

that the intense Raman spectra of the biomarker appear only on the AgNP@BP SERS substrate and not on bare Si substrates. In order to identify the detection limit, Raman signals were recorded with varying concentrations from 1000 pM to 10 fM for both IL-3 and PCT. However, the spectra of the biomarkers were observable only up to 1 pM for IL-3 and 100 fM for PCT, which are the LODs of these two biomarkers on the AgNP@BP SERS substrate.

Clinically, it has been proven that the level of biomarkers present in the infected human body is in the pg mL^{-1} range (~pM concentration), suggesting that the reported LODs on the AgNP@BP SERS substrate can provide three-digit accuracy. This is sensitive enough and more than sufficient for the early detection of the elevated IL-3 and PCT levels in the blood caused by sepsis.[23] The enhancement factor (EF) of the SERS substrate was calculated using the three intense Raman peaks of IL-3 and PCT, appearing at 620, 1366, and 1655 cm^{-1}, where the EF values corresponding to different concentrations of the biomarkers were calculated and are listed in Tables ST5 and ST6.† The obtained average EF values calculated for IL-3 and PCT were as high as ~2.3 × 10^{14} and ~4.5 × 10^{14}, respectively. Table ST7† summarizes the average EF and LODs for all three sepsis biomarkers (LPS, IL-3, and PCT) detected using the AgNP@BP SERS platform.

To the best of our knowledge, this is the first scientific report on the Raman spectra of IL-3 and PCT. Hence, it requires the identification of the vibrational modes corresponding to the observed Raman peaks. The prominent characteristic Raman vibrational peaks of IL-3 and PCT corresponding to 1 pM concentration are compared in Fig. 3a, whereas all of the observed Raman modes are summarized in Table 2. The phonon band assignment of the Raman peaks, and the identification of the signature peaks of the IL-3 and PCT protein structure are challenging tasks. Both biomarkers contain the same building blocks of amino acids with multiple variations in sequence. Hence, they end up interfering with the signature peaks, originating from the structural anomalies.

The amino acid sequence of IL-3 is as follows:[50,51]

*MSRLPVLLLLQLLVRPGLQAPMTQTTPLKTSWVNCSNMIDEIITH
LKQPPLPLLDFNNLNGEDQDILMENNLRRPNLEAFNRAVKSLQNASA
IESILKNLLPCLPLATAAPTRHPIHIKDGDWNEFRRKLTFYLKTLENAQ
AQQTTLSLAIF*

Whereas, the amino acid sequence of PCT is:[52,53]

*APFRSALESSPADPATLSEDEARLLLAALVQDYVQMKASELEQEQ-
EREGSSLDSPRSKRCGNLSTCMLGTYTQDFNKFHTFPQTAIGVGAP-
GKKRDMSSD LERDHRPHVS MPQNAN*

The origin of the Raman peaks (Fig. 3a) of IL-3 and PCT were identified and are listed in Table 2 by comparing the signals with the previously reported Raman spectra of amino acids.[54–56] For instance, the intense Raman peaks that are common for both IL-3 and PCT are observed at 620, 779, 1130, 1187, 1316, 1370, 1513, 1577, and 1655 cm^{-1}, and are the primary characteristics of the amino acids. Common Raman peaks of low intensity are observed for both IL-3 and PCT at ~896, 991, 1096, 1279, 1423, and 1551 cm^{-1},

originating from the amino acids. The observed Raman peak positions of the biomarkers may have perturbations in the peak positions. They may not match exactly with the reported peak positions of the isolated amino acids, as they exist within a long chain of the protein biomarker. In the low energy region, prominent Raman peaks are also present in matching positions (PCT: 81 cm^{-1}, 144 cm^{-1}, and 169 cm^{-1}; IL-3: 79 cm^{-1}, 144 cm^{-1}, and 170 cm^{-1}), originating from the structural vibrations of the short-range identical amino acid sequence.

To identify the Raman *signature modes* of IL-3 and PCT, the spectra (Fig. 3a) were compared in four different ranges, *i.e.*, 50–360 cm^{-1} (Fig. 3b), 550–1000 cm^{-1} (Fig. 3c), 1000–1400 cm^{-1} (Fig. 3d) and 1400–1900 cm^{-1} (Fig. 3e). The Raman signature peaks of IL-3 and PCT are marked in Fig. 3b–e with dotted and solid vertical lines, respectively, whereas, all the signature Raman modes are tabulated in Table ST8.† For instance, a few distinguished low frequency (<350 cm^{-1}) Raman peaks are observed for PCT, such as 122, 170, 229, 203, and 299 cm^{-1}, which are not observed in IL-3. Similarly, the Raman peaks at 65, 92, 118, 177, 221, 265, 292, 347 cm^{-1} are observed in IL-3 but not in the Raman spectra of PCT. Such low energy Raman peaks may originate from the complete structural vibration, and can be considered as the signature Raman modes of IL-3 and PCT. Apart from the low energy Raman modes, a few distinguished high energy (>500 cm^{-1}) Raman peaks are also observed such as 579, 681, 702, 919, 1111, 1285, 1406, 1739, 1752 and 1798 cm^{-1} for IL-3 and 740, 803, 1100, 1228, 1254, 1692, 1807, 1824, 1841 and 1888 cm^{-1} for PCT, which helps to identify the biomarkers precisely. The high energy signature Raman modes of the biomarkers may have originated owing to the long or short-range structural deformation of the long-chain proteins.

In order to confirm the SERS capability of the developed AgNP@BP substrate for the detection of sepsis biomarkers (PCT and IL-3) in spiked clinical samples, solutions of the biomarkers with varying concentrations were prepared in sterile human serum to mimic the real serum sample.[57–60] The as-prepared spiked biomarker samples were drop-casted onto the fabricated SERS substrate, and kept for vacuum drying for two hours. The Raman spectra were recorded using a very low power (<2 mW) laser irradiation to avoid any kind of possible degradation of the molecular structure. The Raman spectra of the IL-3 and PCT in the spiked clinical samples are shown in Fig. 4a and b, where the prominent Raman spectral features were observed in solutions with concentrations as low as 1 pM and 100 fM for IL-3 and PCT, respectively. Such low LOD of both biomarkers obtained in the spiked clinical samples are similar to the obtained LOD of the pure biomarkers (Fig. 2a and b), which establishes the detection capability of the developed AgNP@BP SERS substrate for spiked clinical samples. The identification of biomarkers in clinical samples through SERS is one of the major limitations for the diagnosis of sepsis due to the presence of indistinguishable Raman peaks from several other biomolecules present in the sample. However, the
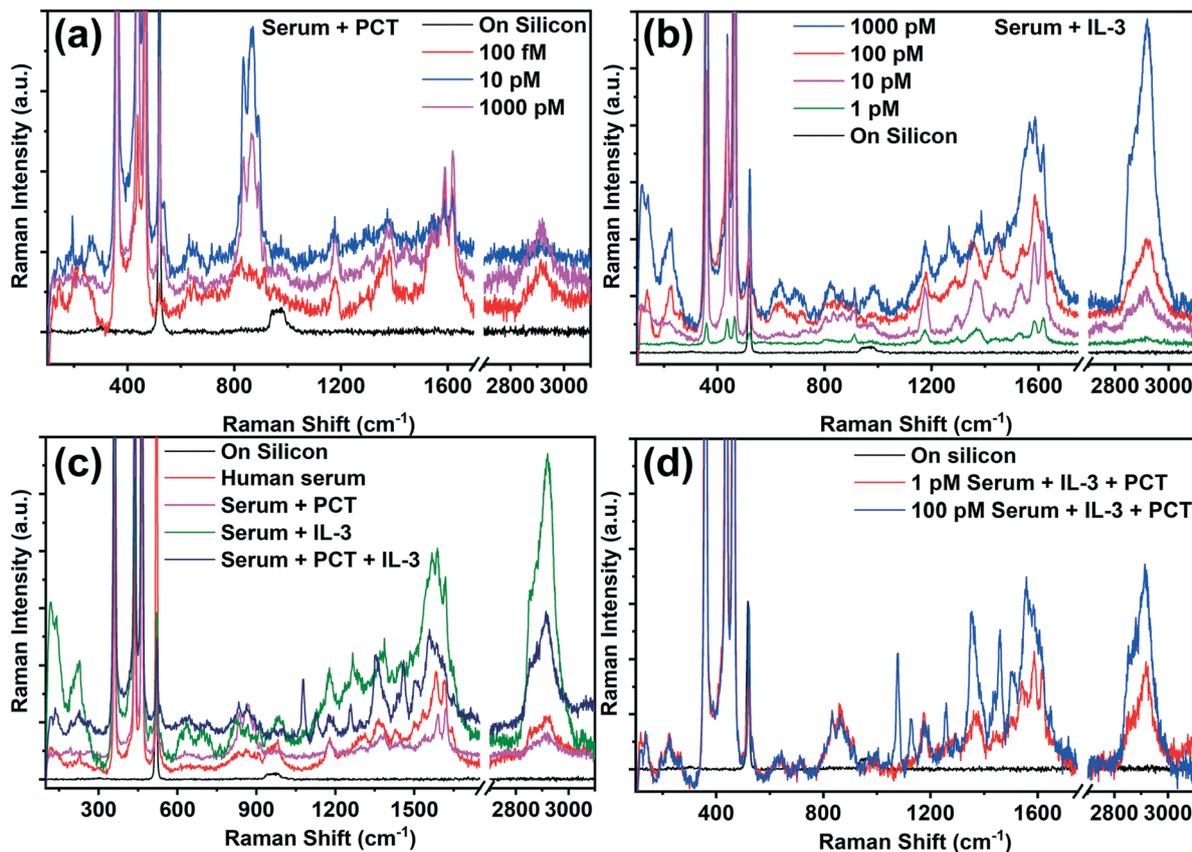
Fig. 4 Raman spectra of the clinical sample prepared in sterile human serum. Raman spectra of (a) PCT and (b) IL-3 in clinical sample with varying concentrations; (c) comparative Raman spectra of sterile human serum, serum_PCT, serum_IL-3, and serum_PCT_IL-3; (d) the Raman spectra of the clinical samples with varying concentrations, where both PCT and IL-3 are simultaneously present.

established signature Raman modes of the sepsis biomarkers (Table ST8†) help us to identify and distinguish the presence of biomarkers in the spiked clinical samples. The calculated SERS EF was obtained on the order of $\sim10^{14}$ as well, *i.e.*, similar to that of the pure biomarker sample. The in-depth analysis of the Raman spectra of the spiked clinical samples was performed by rigorous Lorentzian fitting to identify all of the possible Raman peaks of the biomarkers. The obtained Raman peaks of PCT and IL-3 in the spiked clinical samples are listed in Table ST9,† which matches well with the Raman peaks observed for the pure biomarkers. By comparing the Raman spectra of the spiked clinical samples, it was observed that a strong peak at ~2900 cm^{-1} is present in the case of IL-3, while the same is weak for PCT. Thus, the presence of the Raman peak at ~2900 cm^{-1} significantly denoted the presence of IL-3 in the spiked clinical sample. Such strong peak can be considered as the signature Raman peak of IL-3. To distinguish the Raman modes of the biomarkers from the sterile human serum, Fig. 4c compares the Raman spectra of IL-3, PCT, and serum along with the spiked clinical sample, where both the biomarkers are present simultaneously. As shown in Fig. 4a and b, the Raman peak at ~2900 cm^{-1} has a strong intensity in the case of the IL-3 and mixed (IL-3 + PCT) samples. This further confirmed the Raman peak at ~2900 cm^{-1} as a signature mode of IL-3, in addition to the

previously identified signature Raman modes. Here, it is worthy to note that the Raman peak at ~2900 cm^{-1} is not observed with nearly as strong intensity for the pure biomarkers, although a small peak is observed in that range for IL-3 (Fig. 3b). The possible Raman peaks of the sterile human serum and the corresponding origin of such Raman modes were obtained by analyzing the Raman spectra of sterile human serum (Fig. 4c). The results are listed in Table ST9,† where it was observed that most of the Raman peaks appear in the range of 850–1700 cm^{-1}. The origin of such high energy Raman modes was mainly due to the presence of several proteins and their amino acid building blocks, as mentioned in Table ST10.† Surprisingly, in the case of sterile human serum, no such low energy Raman peak is observed. This becomes an added advantage for the identification of biomarkers in spiked clinical samples, as most of the signature Raman modes of the biomarkers lie in the low energy range (<400 cm^{-1}). Although it can be concluded that the identification of sepsis biomarkers in a spiked clinical sample is possible, the detection of the biomarkers in the presence of each other, *i.e.*, in a mixed state is crucial. To separate the peaks of the biomarkers in the spiked clinical sample, where both of the biomarkers are present, the Raman spectra of the biomarkers in the mixed state for different concentrations were recorded (Fig. 4d). The Raman

spectra of the mixed biomarkers suggests that the presence of the strong Raman peak at ~2900 cm^{-1} confirms the presence of IL-3. Meanwhile, the low frequency Raman modes help to identify the distinct biomarkers from each other. All of the possible Raman peaks of the mixed biomarkers in the clinical samples were analyzed and are listed in Table ST10,† where the origin of each Raman peak was assigned to sterile human serum, IL-3 and PCT according to their signature Raman modes. For instance, the Raman modes observed at 114, 135, 194, 221, and 268 cm^{-1} solely originated from IL-3. These peaks were not observed for PCT nor for sterile human serum, and matched well with the previously identified signature Raman modes of IL-3 (Table ST9†). In a similar fashion, the Raman modes observed at 122, 228 cm^{-1} were observed in the case of PCT only, which are also the signature Raman modes of PCT. Along with the low frequency Raman modes, several other high frequency signature Raman modes of the biomarkers were identified, as mentioned in Table ST10.† Such prominent identification of the distinct Raman peaks for both the biomarkers in the spiked clinical samples, having LOD values as low as 100 fM (for PCT) and 1 pM (for IL-3), confirms the specificity and sensitivity of the developed SERS protocol for the detection of sepsis biomarkers. Thus, an in-depth analysis of the IL-3 and PCT Raman spectra confirmed that the developed SERS substrate may have great potential for immediate application for the detection of ultralow amounts of sepsis biomarkers. This may predict the possibility of septic shock in the amateur stage to prevent deaths caused in septic shock. Such ultrasensitive and stable AgNP@BP flake may also be useful for the development of layered BP based sensors, actuators, and optoelectronic devices.

Conclusions

In summary, the ultrasensitive detection of prognostic and diagnostic biomarkers of sepsis has been established using the AgNP@BP SERS platform. A one-step protocol has been optimized for developing a highly stable BP-based SERS substrate having a uniform distribution of AgNPs. The developed AgNP@BP SERS substrate demonstrates the ultrasensitive detection of sepsis biomarkers, i.e., LPS, IL-3, and PCT, where the limit of detection (LOD) value was as low as 1 nM, 1 pM and 100 fM with an enhancement factor as high as on the order of ~10^{14} for LPS, IL-3 and PCT, respectively. The detection of sepsis biomarkers was demonstrated for the spiked clinical samples as well. All of the possible signature Raman modes of IL-3 and PCT were identified and reported for the first time. Thus, for the detection of prognostic and diagnostic biomarkers of sepsis using the same sensing platform, the developed AgNP@BP SERS substrate may pave a path towards the rapid and early detection of sepsis biomarkers. The main advantage of Raman-based diagnostics over state-of-art fluorescence

diagnostics is its signal selectivity to molecular structure. Hence, it is considered as a fingerprint technique and provides flexibility for the real-time monitoring of the disease condition. Hence, the immediate proposition is to establish a Raman library, identifying the signature peaks of various biomarkers. This is the key in distinguishing various biomarkers having molecular structures of close similarities, and would allow for greater speed, accuracy, online monitoring, and multiplexity during diagnosis.

Author contributions

Anirban Kundu: main conceptualization, methodology, experiment perform, data analysis, original manuscript writing, reviewing & editing; Renu Rani: data curation, reviewing; Anas Ahmad: biomarkers solution preparation, reviewing; Ajay Kumar: writing; Mamta Raturi: writing; Tanya Gupta: data curation; Rehan Khan: conceptualization, writing – reviewing and editing, Kiran Shankar Hazra: supervision, conceptualization, writing – reviewing and editing.

Conflicts of interest

There are no conflicts to declare.

Acknowledgements

References

1 R. D. Schachter and S. Finfer, *Recognizing Sepsis as a Global Health Priority — A WHO Resolution*, 2017, pp. 414–417.

2 C. Fleischmann, *et al.*, Assessment of global incidence and mortality of hospital-treated sepsis current estimates and limitations, *Am. J. Respir. Crit. Care Med.*, 2016, **193**, 259–272.

3 X. Hou, *et al.*, Vitamin lipid nanoparticles enable adoptive macrophage transfer for the treatment of multidrug-resistant bacterial sepsis, *Nat. Nanotechnol.*, 2020, **15**(1), 41–46.

4 R. S. Hotchkiss, L. L. Moldawer, S. M. Opal, K. Reinhart and J. Vincent, Sepsis and septic shock, *Nat. Rev. Dis. Primers*, 2016, **2**(1), 1–21.

5 G. L. Lin, J. P. McGinley, S. B. Drysdale and A. J. Pollard, Epidemiology and Immune Pathogenesis of Viral Sepsis, *Front. Immunol.*, 2018, **9**, 2147.

6 N. Chen, et al., Epidemiological and clinical characteristics of 99 cases of 2019 novel coronavirus pneumonia in Wuhan, China: a descriptive study, Lancet, 2020, 395, 507–513.

7 F. Zhou, et al., Articles Clinical course and risk factors for mortality of adult inpatients with COVID-19 in Wuhan, China: a retrospective cohort study, Lancet, 2020, 6736, 1–9.

8 X. Y. Shao, et al., Rapid and Sensitive Lateral Flow Immunoassay Method for Procalcitonin (PCT) Based on time-resolved immunochromatography, Sensors, 2017, 17(3), 480.

9 A. Belushkin, et al., Rapid and Digital Detection of Inflammatory Biomarkers Enabled by a Novel Portable Nanoplasmonic Imager, Small, 2020, 16(3), 1906108.

10 S. Kumar, S. Tripathy, A. Jyoti and S. G. Singh, Recent advances in biosensors for diagnosis and detection of sepsis: A comprehensive review, Biosens. Bioelectron., 2019, 124, 205–215.

11 A. H. Nguyen, Y. Shin and S. J. Sim, Development of SERS substrate using phage-based magnetic template for triplex assay in sepsis diagnosis, Biosens. Bioelectron., 2016, 85, 522–528.

12 M. M. Guido, et al., In vitro diagnosis of sepsis: a review, Pathol. Lab. Med. Int., 2016, 8, 1–14.

13 S. Riedel and K. C. Carroll, Laboratory Detection of Sepsis Biomarkers and Molecular Approaches, Clin. Lab. Med., 2013, 33, 413–437.

14 G. Polat, R. A. Ugan, E. Cadirci and Z. Halici, Sepsis and Septic Shock: Current Treatment Strategies and New Approaches, Eurasian J. Med., 2017, 49(1), 53–58.

15 S. Haydar, M. Spanier, P. Weems, S. Wood and T. Strout, Comparison of QSOFA score and SIRS criteria as screening mechanisms for emergency department sepsis, Am. J. Emerg. Med., 2017, 35, 1730–1733.

16 J. D. Faix, Biomarkers of sepsis, Infect. Chemother., 2013, 46(1), 23–36.

17 S. Y. Cho and J. H. Choi, Biomarkers of Sepsis, Infect. Chemother., 2014, 46, 1–12.

18 J. Min, et al., Integrated Biosensor for Rapid and Point-of-Care Sepsis Diagnosis, ACS Nano, 2018, 12, 3378–3384.

19 P. A. Mosier-Boss, Review on SERS of bacteria, Biosensors, 2017, 7, 51.

20 P. Xie, et al., Highly sensitive detection of lipopolysaccharides using an aptasensor based on hybridization chain reaction, Sci. Rep., 2016, 6(29524), 1–8.

21 C. Erridge, E. Bennett-Guerrero and I. R. Poxton, Structure and function of lipopolysaccharides, Microbes Infect., 2002, 4, 837–851.

22 G. F. Weber, et al., Interleukin-3 amplifies acute inflammation and is a potential therapeutic target in sepsis, Science, 2015, 347(6227), 1260–1265.

23 J. Min, et al., Integrated Biosensor for Rapid and Point-of-Care Sepsis Diagnosis, ACS Nano, 2018, 12(4), 3378–3384.

24 A. L. Vijayan, et al., Procalcitonin: a promising diagnostic marker for sepsis and antibiotic therapy, J. Intensive Care, 2017, 5(1), 1–7.

25 S. E. J. Weitkamp, Procalcitonin versus C-reactive protein : review of kinetics and performance for diagnosis of neonatal sepsis, J. Perinatol., 2019, 39(7), 893–903.

26 A. Hakeem, A. Mohsen and B. A. Kamel, Predictive values for procalcitonin in the diagnosis of neonatal sepsis, Electron. Physician, 2015, 7(4), 1190–1195.

27 Q. Cai, et al., Boron Nitride Nanosheets Improve Sensitivity and Reusability of Surface Enhanced Raman Spectroscopy, Angew. Chem., 2016, 128(29), 8545–8549.

28 X. Song, et al., Plasmon-Free Surface-Enhanced Raman Spectroscopy Using Metallic 2D Materials, ACS Nano, 2019, 13(7), 8312–8319.

29 J. Li, W. Zhang, H. Lei and B. Li, Ag nanowire / nanoparticle-decorated MoS 2 monolayers for surface-enhanced Raman scattering applications, Nano Res., 2018, 11(4), 2181–2189.

30 Q. Guo, et al., Black Phosphorus Mid-Infrared Photodetectors with High Gain, Nano Lett., 2016, 16(7), 4648–4655.

31 K. Chen, C. Yuen, Y. Aniweh, P. Preiser and Q. Liu, Towards ultrasensitive malaria diagnosis using surface enhanced Raman spectroscopy, Sci. Rep., 2016, 6, 20177.

32 J. T. Walsh, D. Ph, M. R. Glucksberg and D. Ph, Progress Toward an In Vivo Surface-Enhanced Raman Spectroscopy Glucose Sensor, Diabetes Technol. Ther., 2008, 10(4), 257–265.

33 F. Mos, T. Takamura and A. Sandhu, Laser Power Dependent Optical Properties of MoS2, J. Nanosci. Nanotechnol., 2015, 15(9), 6843–6846.

34 Y. Yang, L. Chen, M. Ji and H. Hospital, Stimulated Raman scattering microscopy for rapid brain tumor histology, J. Innovative Opt. Health Sci., 2017, 10, 1–12.

35 M. Xia, A Review on Applications of Two-Dimensional Materials in Surface-Enhanced Raman Spectroscopy, Int. J. Spectrosc., 2018, 4861472.

36 A. Kundu, R. Rani and K. S. Hazra, Controlled nanofabrication of metal-free SERS substrate on few layered black phosphorus by low power focused laser irradiation, Nanoscale, 2019, 11, 16245–16252.

37 X. Ge, Z. Xia and S. Guo, Recent Advances on Black Phosphorus for Biomedicine and Biosensing, Adv. Funct. Mater., 2019, 29, 1900318.

38 Z. Liu, et al., A two-dimensional fingerprint nanoprobe based on black phosphorus for bio-SERS analysis and chemo-photothermal therapy, Nanoscale, 2018, 10, 18795–18804.

39 M. Liang, et al., Silver-Laden Black Phosphorus Nanosheets for an Efficient In Vivo Antimicrobial Application, Small, 2020, 16, 1905938.

40 J. Ouyang, et al., Two dimensional semiconductors for ultrasound-mediated cancer therapy: The case of black phosphorus nanosheets, Chem. Commun., 2018, 54, 2874–2877.

41 W. Lei, et al., Bandgap- and Local Field-Dependent Photoactivity of Ag/Black Phosphorus Nanohybrids, ACS Catal., 2016, 6, 8009–8020.

42 X. Fan, et al., Amperometric sensor for dopamine based on surface-graphenization pencil graphite electrode prepared by

in-situ electrochemical delamination, *Microchim. Acta*, 2019, **186**, 324.

43 R. V. Devi, M. Doble and R. S. Verma, Biosensors and Bioelectronics Nanomaterials for early detection of cancer biomarker with special emphasis on gold nanoparticles in immunoassays / sensors, *Biosens. Bioelectron.*, 2015, **68**, 688–698.

44 X. Cao, Z. Wang, L. Bi and J. Zheng, Label-Free Detection of Human Serum Using Surface-Enhanced Raman Spectroscopy Based on Highly Branched Gold Nanoparticle Substrates for Discrimination of Non-Small Cell Lung Cancer, *J. Chem.*, 2018, **2018**, 9012645.

45 H. Huang, *et al.*, Black phosphorus: a two-dimensional reductant for in situ nanofabrication, *npj 2D Mater. Appl.*, 2017, **1**, 1–8.

46 F. Alsaffar, *et al.*, Raman Sensitive Degradation and Etching Dynamics of Exfoliated Black Phosphorus, *Sci. Rep.*, 2017, **7**, 44540.

47 T. Zhang, *et al.*, Degradation Chemistry and Stabilization of Exfoliated Few-Layer Black Phosphorus in Water, *J. Am. Chem. Soc.*, 2018, **140**, 7561–7567.

48 J. V. Trueblood, *et al.*, Heterogeneous Chemistry of Lipopolysaccharides with Gas-Phase Nitric Acid : Reactive Sites and Reaction Pathways, *J. Phys. Chem. A*, 2016, **120**, 6444–6450.

49 C. N. Kotanen, L. Martinez, R. Alvarez and J. W. Simecek, Sensing and Bio-Sensing Research Surface enhanced Raman scattering spectroscopy for detection and identification of microbial pathogens isolated from human serum, *Sens. Bio-Sens. Res.*, 2016, **8**, 20–26.

50 Y. Feng, B. K. Klein and C. A. McWherter, Three-dimensional solution structure and backbone dynamics of a variant of human interleukin-3, *J. Mol. Biol.*, 1996, **259**, 524–541.

51 D. L. Urdal, *et al.*, Molecular Characterization of Colony-Stimulating Factors and Their Receptors: Human Interleukin-3, *Ann. N. Y. Acad. Sci.*, 1989, **554**, 167–176.

52 J. A. M. Hubbard, *et al.*, Solution structures of calcitonin-gene-related-peptide analogues of calcitonin-gene-related peptide and amylin, *Biochem. J.*, 1991, **275**, 785–788.

53 J. B. Petermann, W. Born, J. Y. Chang and J. A. Fischer, Identification in the human central nervous system, pituitary, and thyroid of a novel calcitonin gene-related peptide, and partial amino acid sequence in the spinal cord, *J. Biol. Chem.*, 1987, **262**, 542–545.

54 Y. Wang, M. Salehi, M. Schütz, K. Rudi and S. Schlücker, Microspectroscopic SERS detection of interleukin-6 with rationally designed gold/silver nanoshells, *Analyst*, 2013, **138**, 1764–1771.

55 G. Zhu, X. Zhu, Q. Fan and X. Wan, Raman spectra of amino acids and their aqueous solutions, *Spectrochim. Acta, Part A*, 2011, **78**, 1187–1195.

56 J. M. Benevides, S. A. Overman and G. J. Thomas Jr, Raman Spectroscopy of Proteins, *Curr. Protoc. Protein Sci.*, 2004, **33**, 17–18.

57 A. H. Nguyen, Y. Shin and S. J. Sim, Development of SERS substrate using phage-based magnetic template for triplex assay in sepsis diagnosis, *Biosens. Bioelectron.*, 2016, **85**, 522–528.

58 L. Tang and J. Casas, Quantification of cardiac biomarkers using label-free and multiplexed gold nanorod bioprobes for myocardial infarction diagnosis, *Biosens. Bioelectron.*, 2014, **61**, 70–75.

59 B. Zhang, A. W. Morales, R. Peterson, L. Tang and J. Y. Ye, Label-free detection of cardiac troponin I with a photonic crystal biosensor, *Biosens. Bioelectron.*, 2014, **58**, 107–113.

60 R. Sharma, *et al.*, Label-free electrochemical impedance biosensor to detect human interleukin-8 in serum with sub-pg/ml sensitivity, *Biosens. Bioelectron.*, 2016, **80**, 607–613.

61 H. Chaudhry, J. Zhou, Y. Zhong, M. M. Ali, F. McGuire, P. S. Nagarkatti and M. Nagarkatti, Role of Cytokines as a Double-edged Sword in Sepsis, *In Vivo*, 2013, **27**, 669–684.

62 M. L. Steinhauser, C. M. Hogaboam, A. Matsukawa, N. W. Lukacs and R. M. Strieter, Chemokine C10 Promotes Disease Resolution and Survival in an Experimental Model of Bacterial Sepsis, *Infect. Immun.*, 2000, **68**, 6108–6114.

63 J. Charchaflieh, J. Rushbrook, S. Worah and M. Zhang, Activated Complement Factors as Disease Markers for Sepsis, *Dis. Markers*, 2015, **2015**, 382463.

64 D. D. Danikas, M. Karakantza, G. L. Theodorou, G. C. Sakellaropoulos and C. A. Gogos, Prognostic value of phagocytic activity of neutrophils and monocytes in sepsis. Correlation to CD64 and CD14 antigen expression, *Clin. Exp. Immunol.*, 2008, **154**, 87–97.

65 K. Reinhart, M. Bauer, N. C. Riedemann and C. S. Hartog, New Approaches to Sepsis: Molecular Diagnostics and Biomarkers, *Clin. Microbiol. Rev.*, 2012, **25**, 609–634.

66 S. Newton, *et al.*, *NIH Public Access*, 2008, **5**, 375–383.

67 H. Lim, *et al.*, Synthesis of Uniformly Sized Mesoporous Silver Films and Their SERS Application, *J. Phys. Chem. C*, 2020, **124**, 23730–23737.

68 H. Lim, *et al.*, A mesopore-stimulated electromagnetic nearfield: electrochemical synthesis of mesoporous copper films by micelle self-assembly, *J. Mater. Chem. A*, 2020, **8**, 21016–21025.

69 G. Kwon, *et al.*, Nanoporous cellulose paper-based SERS platform for multiplex detection of hazardous pesticides, *Cellulose*, 2019, **26**, 4935–4944.